THE JOURNAL OF PHYSICAL CHEMISTRY B

Article

pubs.acs.org/JPCB

Modeling of the Role of Conformational Dynamics in Kinetics of the Antigen–Antibody Interaction in Heterogeneous Phase

David Giménez-Romero,[†] Miguel A. González-Martíne,[†] Maria-José Bañuls,[†] Isidro S. Monzó,[‡] Rosa Puchades,[†] and Ángel Maquieira*[,†]

[†]Instituto de Reconocimiento Molecular & Desarrollo Tecnológico, Universidad Politécnica de Valencia, Camino de Vera s/n, 46022 Valencia, Spain

[‡]Departament de Química Física, Universitat de València, C/Dr Moliner, 50, 46100, Burjassot, València, Spain

ABSTRACT: A novel approach that may potentially be used to study biomolecular interactions including the simultaneous determination of structural and kinetic binding parameters is described in this Article for the first time. It allows a rigid distinction between the possible reaction mechanisms of biomolecular recognition, induced fit and conformational selection. The relative importance of the two pathways is determined not by comparing rate constants but the structural aspects of the interaction instead. So the exact location of antigen molecules with respect to the capture antibody is depicted experimentally, avoiding the use of X-ray crystallography. The proposed pattern is applied to study the anti-BSA Immunoglobulin G (IgG)-free Bovine Serum Albumin (BSA) interaction, in which IgG is anchored on a silicon chip sensing surface in an oriented manner. The exact location of the receptor with respect to the ligand was monitored during the binding process, thus drawing the full reaction scheme. IgG forms an asymmetric $(FabBSA)_2$ complex with BSA molecules, even though it has two identical fragment antigen binding arms. This is thought to be due to steric hindrance caused by the binding of the first BSA molecule. Furthermore, the proposed model allows one to characterize reaction intermediates without the need of isolating them. These intermediates not characterized in situ so far are the keystone to understand how antibodies are able to identify antigens.

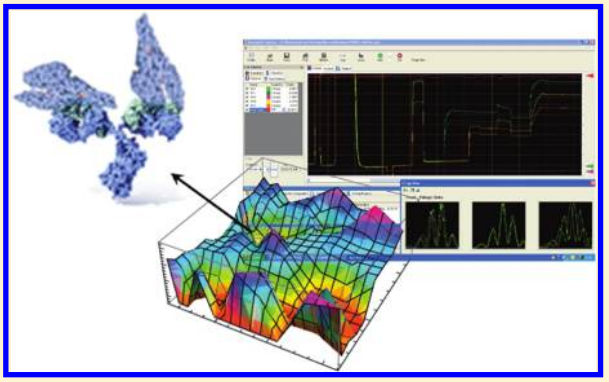

INTRODUCTION

Some of the outstanding questions in the fields of biology and life sciences remain unsolved as a result of our limited knowledge of the function, behavior, and concerted interaction of significant biomolecules. Interaction studies at the molecular level for the determination of affinity, conformational changes, and kinetic rates are important for understanding biological reactions and for the development of new drugs. Furthermore, recognition of biomolecules binding to surface immobilized specific probes is central for elucidating complex pathways in biological systems.[1] Immunoreagents and catalytic antibodies development, cell adhesion, and polymer–macromolecule boundary are also some of the hot research areas related to biomolecular interactions. Hence, the novel knowledge from these interactions provides advances in mechanisms to impact fundamental understandings in chemistry.

Protein ligand molecular recognition is determined by the structure and dynamics of both, but it is difficult to directly assess the role of each player. Unfortunately, while experimental methods can clearly delineate the kinetic aspects of a given biomolecular interaction, it is much more difficult to pinpoint the induced conformational changes and, therefore, their role in biomolecular interactions. Considerable effort has been expended in assessing the detailed mechanism by which ligand binding and conformational changes are coupled.[2] Two limiting mechanisms are usually considered:[3] (i) induced fit,[4] which implies that the binding reaction itself induces conformational changes leading to a better complementarity between epitope and paratope, that is, an initial complex formation followed by a conformational change in the complex, and (ii) conformational selection,[5] where the antibody simply selects the antigen molecules whose epitope is already in a fitting conformational state,[6] or, in the reciprocal case, the antigen selects the antibody that happens to be in the complementary conformation.[7] So far, recent studies and experiments are still trying to find a rigid distinction between both models.

Biomolecular interactions are studied by circular dichroism, NMR, X-ray diffraction, atomic force microscopy, electrochemistry, etc. Microarray technology facilitates the sensing of multiple probe-target interactions in parallel, in heterogeneous format. Hence, several techniques have also been applied for the label-free detection of biomolecular interactions, such as ellipsometry (single wavelength or spectroscopic),[8,9] quartz crystal microbalance,[10] waveguide grating coupler,[11] or plasmon-based devices (surface plasmon resonance (SPR) and

Received: February 28, 2012
Revised: April 20, 2012
Published: April 23, 2012

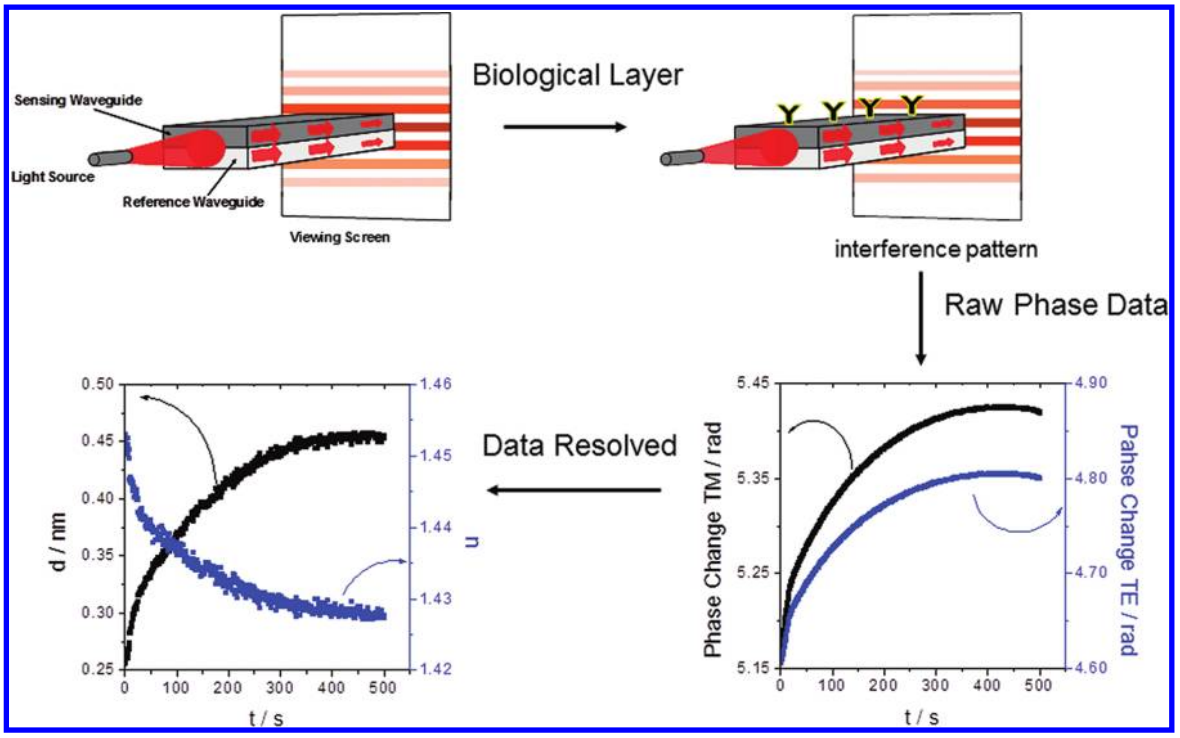

Figure 1. Schematic of a DPI sensor chip and the interference pattern produced when light is applied onto the side of a chip (from Cross et al.[15]).

photonic structures).[12] All of these techniques allow the mechanisms of biomolecular interactions to be understood only by the knowledge of rate and equilibrium constants.[13,14]

Binding of biomolecules to surfaces and interaction with targets displayed in a label-free and real-time manner is no longer reached by few ways. Dual polarization interferometry (DPI) allows this, which is based on a dual waveguide interferometric effect.[15] Figure 1 shows a schematic of a DPI sensor. Light from a laser is passed through the sandwiched waveguide structure, and an interference pattern is detected on the opposing side by a CCD camera. The phase shift of the fringes (TM and TE) is recorded in real time, and data are resolved, where only one value of thickness and absolute refractive index at any given time-point t will satisfy Maxwell's equations of electromagnetism for both TM and TE polarizations. Differences in the waveguide mode dispersion between the transverse electric and transverse magnetic modes allow unique solutions for adlayer thickness and refractive index to be determined. Thus, this technique provides precise measurements, simultaneously and in real time, enabling details of the structure and function of biomolecules to be elucidated. High-quality information on the orientation, distortion, and efficiency of immobilization procedures as well as the interaction event of interest is obtained.

The technique has been previously verified using standard protein systems and by comparing the data with X-ray crystallography and neutron reflection techniques. The precision of the thickness measurements taken was of the order of 40 pm.[15] Thus, DPI has proven to be a powerful technique for characterizing structural dimensions of proteins[16] and has recently been shown to be an instrumental tool for characterization of membrane/liposome structure and mimetics.[17−19]

On the other hand, the refractive index measurements have been verified using ellipsometric determination with accuracy of 10^{-3} refractive index units.[15] DPI data are also in good agreement with the well-established SPR data.[20] Unlike SPR, which utilizes only the TM mode, DPI takes advantage of measuring both the TM and the TE polarizations.[21] Thus, Maxwell's equations of electromagnetism for a system of uniform multiple dielectric layers are employed to provide the absolute effective index for both the TM and the TE waveguide modes determined from the refractive index and thickness of each layer from each polarization.[15] Changes to the adsorbed layer will result in a change to the effective index of each mode that can satisfy a continuous distribution of thickness and refractive index values with only one unique solution that satisfies both the TM and the TE modes. Accordingly, the use of both polarizations to determine effective refractive index and thickness values is clearly a great advantage over SPR, resonant mirror, resonant waveguide grating, and other optical biosensor techniques that report relative changes of refractive index obtained from only one polarization.[22]

DPI has been mainly used to resolve mechanistic aspects of adsorption processes,[23] layer formation kinetics,[24] and surface polymerization.[25] However, its application to study biomolecular interaction kinetics is limited, and it is based mainly on the determination of thermodynamic parameters, affinity constants, under stationary research conditions.[26]

Accordingly, a novel approach that may potentially be used to study biomolecular interactions including the simultaneous determination of structural and kinetic binding parameters is described in this Article. A model for the numerical simulation of empirical data, measured by DPI while the biomolecular interaction is happening, is here developed. The proposed model is verified by studying the anti-BSA Immunoglobulin G (IgG)-free Bovine Serum Albumin (BSA) interaction, in which the IgG is oriented anchored on a chip sensing surface. This model may allow the experimental signal to be deconvoluted, characterizing reaction intermediates without the need of isolating them. These intermediates have not been characterized in situ so far. So, researchers of both the chemical and the biochemical sciences may benefit from this mechanistic approach.

dx.doi.org/10.1021/jp301953z | J. Phys. Chem. B 2012, 116, 5679−5688

THEORETICAL DESCRIPTION

Usually, the kinetics of antibody−antigen interactions in heterogeneous format is established from the calculation of the average kinetic binding constants. These constants can be estimated by monitoring the ability to form the antibody−antigen complex as the antigen/antibody ratio is increased, as realized here.

The first question to ask before making the empirical determination of the association and dissociation constants is to specify the reaction mechanism of the studied antibody−antigen interaction.

IgG molecules have two identical halves that together form the Y-like shape.[27,28] Each end of the fork contains the antigen binding sites, the fragments antigen-binding (Fab fragments). Hence, these fragments could react in two different ways: the two Fab fragments have identical association constants; and the two Fab fragments have different association constants.

Both hypotheses can be described through the same reaction scheme, because if the two Fab fragments have identical association constants, $k_{2,i}$ is equal to $k_{1,i}$:

$$\mathrm{P_{weak}} + \mathrm{L} \underset{k_{1,-1}}{\overset{k_{11}}{\rightleftharpoons}} \mathrm{P_{weak}{*}L} \underset{k_{1,-2}}{\overset{k_{1,2}}{\rightleftharpoons}} \mathrm{P_{tight}{*}L} \tag{1}$$

$$\mathrm{P_{weak}{*}L} + \mathrm{L} \underset{k_{2,-1}}{\overset{k_{2,1}}{\rightleftharpoons}} \mathrm{P_{2,weak}{*}L} \underset{k_{2,-2}}{\overset{k_{2,2}}{\rightleftharpoons}} \mathrm{P_{2,tight}{*}L} \tag{2}$$

$$\mathrm{P_{tight}{*}L} + \mathrm{L} \underset{k_{2,-1}}{\overset{k_{2,1}}{\rightleftharpoons}} \mathrm{P_{2,weak}{*}L} \underset{k_{2,-2}}{\overset{k_{2,2}}{\rightleftharpoons}} \mathrm{P_{2,tight}{*}L} \tag{3}$$

where P_{weak} and P_{tight} are the weakly and tightly binding conformations of the antibody, and L is the antigen. The mathematical model that describes this reaction scheme is then developed, where it is also connected theoretically to the analytical signals of DPI.

Typically, to detect the presence of conformational selection model, concentration-dependent kinetics experiments are performed, where the conformational interconversion becomes the rate-limiting step at very high ligand concentration. According to the approach proposed here to discern the conformation activity relationship, the same model should simulate both the refractive index and the thickness of molecular scale layers in which the oriented IgG-free BSA interaction takes place when the free antigen amount is increased to guarantee that the BSA concentration is not high enough to distinguish the two limiting mechanisms (induced fit and conformational selection). To assess the certainty of the best-fit values, the same kinetic parameters may explain the time evolution of both refractive index and thickness data when the free antigen amount is increased. The ability to reproduce all of these plots (the evolution of two different analytical signals with the reaction time when the antigen amount is increased; that is, the simultaneous simulation of 10 different plots) is shown to depend on the robustness of the simulation model, and, besides, it allows whether there is a link between variables to be judged.

The system of differential equations for the proposed reaction scheme, eqs 1−3, involves the following expressions:

$$\frac{\mathrm{d}N_{\mathrm{P_{weak}{*}L}}}{\mathrm{d}t} = k_1 N_{\mathrm{P_{weak}}} N_{\mathrm{L}} + k_{-2} N_{\mathrm{P_{tight}{*}L}} - (k_{-1} + k_{-2}) N_{\mathrm{P_{weak}{*}L}} \tag{4}$$

$$N_{\mathrm{P_{weak}}} = N_{\mathrm{P_{weak},0}} - (N_{\mathrm{P_{weak}{*}L}} + N_{\mathrm{P_{tight}{*}L}}) \tag{5}$$

$$\frac{\mathrm{d}N_{\mathrm{P_{2,tight}{*}L}}}{\mathrm{d}t} = k_{2,2} N_{\mathrm{P_{2,weak}{*}L}} - k_{2,-2} N_{\mathrm{P_{2,tight}{*}L}} \tag{6}$$

$$\frac{\mathrm{d}N_{\mathrm{P_{2,weak}{*}L}}}{\mathrm{d}t} = k_{2,1} N_{\mathrm{P_{2,weak}}} N_{\mathrm{L}} + k_{2,-2} N_{\mathrm{P_{2,tight}{*}L}} - (k_{2,-1} + k_{2,2}) N_{\mathrm{P_{2,weak}{*}L}} \tag{7}$$

$$N_{\mathrm{P_{2,weak}}} = (N_{\mathrm{P_{weak}{*}L}} + N_{\mathrm{P_{tight}{*}L}}) - (N_{\mathrm{P_{2,weak}{*}L}} + N_{\mathrm{P_{2,tight}{*}L}}) \tag{8}$$

where it is assumed that the IgG−BSA interaction influences itself following binding regardless of the reached conformation; that is, the association constants of both P_{weak*L} and $P_{tight*L}$ complexes for the second ligand are considered equal, $k_{2,1}$ and $k_{2,2}$.

A consistent set of initial conditions of this reaction scheme is:

$$N^{t=0}_{\mathrm{P_{weak}}} = N_{\mathrm{P_{weak},0}} \tag{9}$$

$$N^{t=0}_{\mathrm{P_{tight}{*}L}} = N^{t=0}_{\mathrm{P_{weak}{*}L}} = 0 \tag{10}$$

$$N^{t=0}_{\mathrm{P_{2,weak}}} = N^{t=0}_{\mathrm{P_{2,weak}{*}L}} = N^{t=0}_{\mathrm{P_{2,tight}{*}L}} = 0 \tag{11}$$

where $N_{Pweak,0}$ is the capture antibody amount.

After defining initial conditions, the system can be easily solved:

$$\begin{aligned} N_{\mathrm{P_{weak}}} = N_{\mathrm{P_{weak},0}} &- \frac{e^{-1/2(k_{1,1}N_{\mathrm{L}}+k_{1,2}+\sqrt{-4k_{1,1}N_{\mathrm{L}}k_{1,2}+(k_{1,1}N_{\mathrm{L}}+k_{1,2})^2})t}\left(-1 + e^{t\sqrt{-4k_{1,1}N_{\mathrm{L}}k_{1,2}+(k_{1,1}N_{\mathrm{L}}+k_{1,2})^2}}\right)k_{1,1}N_{\mathrm{L}}N_{\mathrm{P_{weak},0}}}{\sqrt{-4k_{1,1}N_{\mathrm{L}}k_{1,2} + (k_{1,1}N_{\mathrm{L}} + k_{1,2})^2}} \\ &- N_{\mathrm{P_{weak},0}} e^{-1/2(k_{1,1}N_{\mathrm{L}}+k_{1,2}+\sqrt{-4k_{1,1}N_{\mathrm{L}}k_{1,2}+(k_{1,1}N_{\mathrm{L}}+k_{1,2})^2})t}\left(\frac{k_{1,1}N_{\mathrm{L}}\left(1 - e^{t\sqrt{-4k_{1,1}N_{\mathrm{L}}k_{1,2}+(k_{1,1}N_{\mathrm{L}}+k_{1,2})^2}}\right)}{2\sqrt{-4k_{1,1}N_{\mathrm{L}}k_{1,2} + (k_{1,1}N_{\mathrm{L}} + k_{1,2})^2}}\right. \\ &+ \frac{k_2\left(1 - e^{t\sqrt{-4k_{1,1}N_{\mathrm{L}}k_{1,2}+(k_{1,1}N_{\mathrm{L}}+k_{1,2})^2}}\right) - \sqrt{-4k_{1,1}N_{\mathrm{L}}k_{1,2} + (k_{1,1}N_{\mathrm{L}} + k_{1,2})^2}\left(1 + e^{t\sqrt{-4k_{1,1}N_{\mathrm{L}}k_{1,2}+(k_{1,1}N_{\mathrm{L}}+k_{1,2})^2}}\right)}{2\sqrt{-4k_{1,1}N_{\mathrm{L}}k_{1,2} + (k_{1,1}N_{\mathrm{L}} + k_{1,2})^2}} \\ &\left. + \frac{2e^{1/2(k_{1,1}N_{\mathrm{L}}+k_{1,2}+\sqrt{-4k_{1,1}N_{\mathrm{L}}k_{1,2}+(k_{1,1}N_{\mathrm{L}}+k_{1,2})^2})t}\sqrt{-4k_{1,1}N_{\mathrm{L}}k_{1,2} + (k_{1,1}N_{\mathrm{L}} + k_{1,2})^2}}{2\sqrt{-4k_{1,1}N_{\mathrm{L}}k_{1,2} + (k_{1,1}N_{\mathrm{L}} + k_{1,2})^2}}\right) \end{aligned} \tag{12}$$

dx.doi.org/10.1021/jp301953z | J. Phys. Chem. B 2012, 116, 5679−5688

$$N_{P_{weak}*L} + N_{P_{tight}*L} = \frac{k_{1,1}N_L N_{P_{weak},0}}{(k_{1,1}N_L - k_{2,1}N_L)}(e^{-k_{1,1}N_L t} - e^{-k_{2,1}N_L t}) \quad (13)$$

$$N_{P_{2,weak}*L} = k_{2,1}k_{1,1}N_L^2 N_{P_{weak},0}\left(\frac{e^{-k_{2,2}t}}{(k_{2,1}N_L - k_{2,1})(k_{1,1}N_L - k_{2,2})} + \frac{e^{-k_{1,1}N_L t}}{(k_{1,1}N_L - k_{2,1}N_L)(k_{1,1}N_L - k_{2,2})} - \frac{e^{-k_{2,1}N_L t}}{(k_{1,1}N_L - k_{2,1}N_L)(k_{2,1}N_L - k_{2,2})}\right) \quad (14)$$

$$N_{P_{2,tight}*L} = N_{P_{weak},0}\left(1 + \frac{e^{-k_{2,1}N_L t}k_{1,1}N_L k_{2,2}}{(k_{1,1}N_L - k_{2,1}N_L)(k_{2,1}N_L - k_{2,2})} - \frac{e^{-k_{2,2}t}k_{2,1}N_L k_{1,1}N_L}{(k_{2,1}N_L - k_{2,2})(k_{1,1}N_L - k_{2,2})} - \frac{e^{-k_1 N_L t}k_{2,1}N_L k_{2,2}}{(k_{1,1}N_L - k_{2,1}N_L)(k_{1,1}N_L - k_{2,2})}\right) \quad (15)$$

As the conformation dynamics of the association kinetics is studied, the experimental design favors direct reactions against reverse, because most species in solution are nonlinked BSA molecules, and, besides, the adlayer of immunoglobulin molecules are nonlinked at the beginning of the reaction. Thus, considering Le Chatelier's principle, the dissociation reaction of antigen−antibody complex is hindered when compared to the association reaction at these experimental conditions. Hence, the reverse rates are not considered here to simplify the deduced expressions.

On the other hand, and as shown by eq 13, the $N_{Pweak*L}$ and $N_{Ptight*L}$ values are not a direct solution of this system of differential equations; however, these values can be estimated considering the ratio between both amounts when there is only one Fab fragment that reacts; the equations of this model are not explicit in this Article because of its simplicity. As the reaction of the first Fab fragment is independent of the second reaction, the ratio between $N_{Pweak*L}$ and $N_{Ptight*L}$ may be kept up when the second reaction is considered. Therefore:

$$N_{P_{weak}*L} = \frac{\frac{2k_{1,1}N_L}{(k_{1,1}N_L - k_{2,1}N_L)}\frac{(e^{-k_{1,1}N_L t} - e^{-k_{2,1}N_L t})k_{1,1}N_L N_{P_{weak},0}}{\sqrt{-4k_{1,1}N_L k_{1,2} + (k_{1,1}N_L + k_{1,2})^2}}}{\frac{k_{1,1}N_L - k_{1,2}}{\sqrt{-4k_{1,1}N_L k_{1,2} + (k_{1,1}N_L + k_{1,2})^2}} - \frac{\left(1 + e^{t\sqrt{-4k_{1,1}N_L k_{1,2} + (k_{1,1}N_L + k_{1,2})^2}}\right)}{\left(-1 + e^{t\sqrt{-4k_{1,1}N_L k_{1,2} + (k_{1,1}N_L + k_{1,2})^2}}\right)} + \frac{2e^{-1/2(k_{1,1}N_L + k_{1,2} + \sqrt{-4k_{1,1}N_L k_{1,2} + (k_{1,1}N_L + k_{1,2})^2})t}}{\left(-1 + e^{t\sqrt{-4k_{1,1}N_L k_{1,2} + (k_{1,1}N_L + k_{1,2})^2}}\right)}} \quad (16)$$

$$N_{P_{tight}*L} = \frac{\frac{k_{1,1}N_L N_{P_{weak},0}}{(k_{1,1}N_L - k_{2,1}N_L)}(e^{-k_{1,1}N_L t} - e^{-k_{2,1}N_L t})}{\frac{-k_{1,1}N_L + k_{1,2}}{\sqrt{-4k_{1,1}N_L k_{1,2} + (k_{1,1}N_L + k_{1,2})^2}} - \frac{\left(1 + e^{t\sqrt{-4k_{1,1}N_L k_{1,2} + (k_{1,1}N_L + k_{1,2})^2}}\right)}{\left(1 - e^{t\sqrt{-4k_{1,1}N_L k_{1,2} + (k_{1,1}N_L + k_{1,2})^2}}\right)} + \frac{2e^{-1/2(k_{1,1}N_L + k_{1,2} + \sqrt{-4k_{1,1}N_L k_{1,2} + (k_{1,1}N_L + k_{1,2})^2})t}}{\left(1 - e^{t\sqrt{-4k_{1,1}N_L k_{1,2} + (k_{1,1}N_L + k_{1,2})^2}}\right)}} * \left(\frac{k_{1,1}N_L + k_{1,2}}{\sqrt{-4k_{1,1}N_L k_{1,2} + (k_{1,1}N_L + k_{1,2})^2}} - \frac{\left(1 + e^{t\sqrt{-4k_{1,1}N_L k_{1,2} + (k_{1,1}N_L + k_{1,2})^2}}\right)}{\left(1 - e^{t\sqrt{-4k_{1,1}N_L k_{1,2} + (k_{1,1}N_L + k_{1,2})^2}}\right)} + \frac{2e^{-1/2(k_{1,1}N_L + k_{1,2} + \sqrt{-4k_{1,1}N_L k_{1,2} + (k_{1,1}N_L + k_{1,2})^2})t}}{\left(1 - e^{t\sqrt{-4k_{1,1}N_L k_{1,2} + (k_{1,1}N_L + k_{1,2})^2}}\right)}\right) \quad (17)$$

As commented above, DPI provides sensitive measurements of both thickness and refractive index of adlayers. Hence, the time evolution of each reactive species amount may be connected theoretically to these analytical signals to simulate the experimental data. The most widely used theoretical method for predicting the refractive index of mixtures is the Lorentz−Lorenz relation.[29,30] This equation is generalized for mixtures of noninteracting molecules by the use of the following expression:[31,32]

$$\frac{n^2 - 1}{n^2 + 1} = \frac{4\pi}{3}\sum_i N_i\alpha_i \quad (18)$$

where n is the refractive index, α_i is the polarizability volume per mole for species i, and N_i is the amount of each species estimated form eqs 12−17.

The thickness of the protein layer adsorbed at the sensor (solid)−liquid interface can be estimated by:

$$d = \frac{1}{N_T}\sum_i N_i d_i \quad (19)$$

Here, d is the thickness change of the adlayer, d_i is the height change of the captured ligand (such as antibody or other macromolecule) due to its binding with the receptor i (such as antigen or other ligand), and N_T is the maximum amount of species that can be captured. The determination of the values of d_i allows a structural analysis at the atomic level of reactive species during the biomolecular interaction to be realized, because these values depend inherently on the exact location of antigen molecules with respect to the capture antibody.

It is important to emphasize that $d_{P_{i,weak}*L}$ is different from zero when the limiting mechanism is induced fit, and it is zero

dx.doi.org/10.1021/jp301953z | J. Phys. Chem. B 2012, 116, 5679−5688

when the limiting mechanism is conformational selection, because this last limiting mechanism establishes an intermediate state without receptor−ligand binding. Thus, if the two limiting mechanisms in the two binding sites were due to the conformational selection mechanism, $d_{P_{weak}*L}$ and $d_{P_{2,weak}*L}$ should be equal to zero. However, if the two limiting mechanisms (induced fit and conformational selection) operated the same time depending on which region of the molecule one is focused on, then only one of these values should be zero. Hence, the scenario where the two limiting mechanisms (induced fit and conformational selection) operate the same time in a given macromolecule is also considered here.

Finally, it is important to emphasize that if the reaction scenario is very complex, the kinetic model set forth herein should be modified to take into account this new situation and thus correctly estimate the N_i amounts. Nevertheless, the modeling of DPI data by eqs 18 and 19 should be also applicable to this new situation to discern the conformation activity relationship in biomolecular interactions. The investigation of these complex scenarios will also be important in future work.

EXPERIMENTAL SECTION

Instrument. AnaLight Bio200 dual waveguide interferometer instrument (Farfield Scientific Ltd., Crewe, UK) was used.[15] The instrument accepts a silicon oxynitride sensor chip (dimensions 24 × 5.8 mm), which is comprised of a two-channel integrated dual waveguide Young's interferometer clamped inside a thermostatted block, achieving temperature control within 1 mK. The system has two fluidic interfaces at the sensing surface, 2 μL dead volume each. These are named channel 1 and channel 3, with an additional waveguide reference area, and with channel 2 having a dielectric cover with constant refractive index. The fluidic is managed by means of a double-channel precision syringe pump (Harvard Apparatus PHD 2000 Infusion, Kent, UK) and a dual injection valve. A helium neon laser (λ = 632.8 nm) illuminates the end facet of the chip with a line image applied with a Powell lens. The state of polarization of the input beam is switched between TE and TM, using a ferroelectric liquid crystal (FLC) 1/2 wave plate at typical frequencies of 50 Hz by the digital signal processing chip. The high tolerance to incident beam relative movement is important here as the FLC plate produces small refractive displacements during switching but the output image remains stationary throughout. The diffraction fringe image illuminates a 1024 × 1024 element-imaging device, the output being passed to the DSP unit. The image device output is synchronized with the FLC drive signal and sampled. The relative phase position is updated every 20 ms using a spatial Fourier transform method. These data are transferred to a personal computer, providing real-time results.

Materials, Chemicals, and Operations. Amine-derivatized chips (FB 100, Farfield Scientific Ltd., Crewe, UK), comprised of a silicon oxynitride surface modified to introduce covalently bound amine groups, were used. Biochemicals employed were BSA Fraction V and a polyclonal rabbit anti-BSA whole antiserum, both from Sigma (Madrid, Spain). Sodium periodate and other common chemicals were analytical grade. Water employed in all stages was Milli-Q purified. Carrier solution was phosphate buffered saline (PBS; 10 mM phosphate, 137 mM NaCl, 2.7 mM KCl, pH 7.4), degassed by sonication in a vacuum prior to being introduced in syringe pumps.

The first stage of measurement involved a calibration procedure that allows the exact thickness and refractive index of the waveguide sensor layer to be determined.[15] Complete calibration consists of three stages:[33] signal linearization by injecting 200 μL of EtOH:H_2O 80:20 (w/w) at 100 μL/min followed by stabilization back to PBS baseline at 15 μL/min at the end of injection; chip calibration by registering absolute signal of injected EtOH:H_2O 80:20 (w/w); and bulk calibration by recording signals when flushing pure water.

The real experiment started with the site-directed covalent immobilization of the oriented antibody on the amine chip. That was carried out by dissolving the antiserum in 0.05 M sodium acetate buffer, pH 5.5, and oxidizing it with 0.1 M $NaIO_4$, according to the procedure by Wilson and Nakane.[34] That generates aldehyde groups in the carbohydrate moieties present in the fragment crystallizable region (Fc region) of immunoglobulins, which further condense with amine groups on the chip. The immobilization was carried out by injecting 200 μL of a 50 μg/mL (312 nM) oxidized antibody solution ($M_w \cong$ 160 KDa) in acetate buffer, followed by 50 μL of 4 mg/mL (1.3 mM) $NaBH_4$ in water, to stabilize the imine binding by reduction to amine, both injections at 50 μL/min flow rate.

The binding-association experiments were performed by successive injections of BSA (M_w = 65 KDa) solutions in PBS (250 at 50 μL/min), waiting for a minimum of 7 min between injections, so that dissociation is complete. BSA concentrations ranged from 0.10 to 5.00 μg/mL (1.5−77 nM).

RESULTS AND DISCUSSION

The developed theoretical model was verified by simulating the empirical results of the oriented rabbit IgG polyclonal antibody-free BSA interaction, eqs 12−19. The maximum number of parameters used should be at most equal to the number of data points, but it is preferred that this number is much smaller to minimize errors. So the proposed model may allow the 250 data points to be measured by DPI technique until the steady state is obtained to be simulated. Hence, although high, the number of simulation parameters of the model is acceptable. Furthermore, the simultaneous analysis of two analytical signals guarantees the robustness of the simulation model, because if the model is true, then same kinetic model should reproduce multiple analytical responses. The procedure of simultaneous modeling allows one to improve the accuracy of the simulation parameters because the interference of background noise on the simulation process decreases; the system response is the same for both analytical signals, whereas the noise is random and therefore it counteracts. Thus, this simultaneous modeling helps in spanning parameter space better and reduces simulation error. It also allows whether there is a link between variables to be judged.

To assess the certainty of the best-fit parameter values, the parameters to be used during the simulation of the empirical data may be set to varying environmental features. Thus, it is possible to significantly reduce the relative error of the variables of the proposed model. Accordingly, the general theory is here validated by predicting time evolution of both the refractive index and the thickness of molecular scale layers in which the oriented IgG-free BSA interaction takes place, under dynamic research conditions. Furthermore, the same kinetic parameters may explain the time evolution of both analytical signals as the antigen/antibody ratio is increased. The ability of the proposed model to reproduce all of these plots is shown to depend on the robustness of the model. Also, it finds values for best-fit parameters that minimize errors.

Figure 2 shows how the prediction of the proposed reaction scheme compares well with the experimental data. Accordingly, Table 1 shows the arithmetic mean of residual variances

dx.doi.org/10.1021/jp301953z | J. Phys. Chem. B 2012, 116, 5679−5688

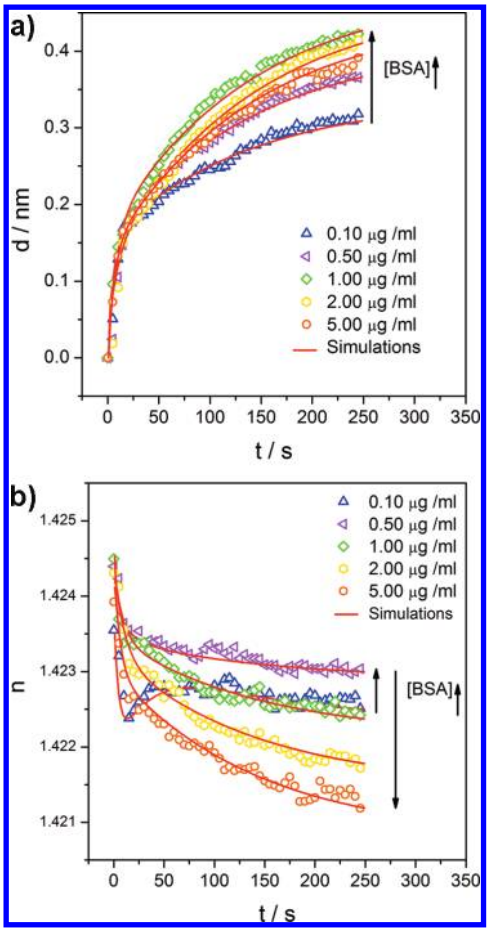

Figure 2. (a) Time evolution curve of the refractive index for the oriented polyclonal IgG-free BSA interaction in PBS (pH 7.4) at 20 °C. (b) Curve of the adlayer thickness. The arrows mean the evolution of the analytic signals as the antigen/antibody ratio increases. All plots show only one point for every five points that are measured.

Table 1. Residual Variances of the Simulations of the Thickness and Refractive Index with the Binding Time for Different Antigen/Antibody Ratios

[BSA], μg/mL	$resVar_{thickness}$, nm^2	$resVar_{refractive\ index}$
0.10	8.46×10^{-5}	14.01×10^{-9}
0.50	14.08×10^{-5}	9.76×10^{-9}
1.00	6.47×10^{-5}	9.19×10^{-9}
2.00	12.41×10^{-5}	7.03×10^{-9}
5.00	3.75×10^{-5}	11.86×10^{-9}

of the thickness simulations is 9.03×10^{-5} nm^2, whereas the arithmetic mean of the variances of the refractive index simulations, considering the same simulation coefficients, is 10.37×10^{-9}.

Table 2 lists the simulation coefficients of the oriented IgG-free BSA interaction when the free antigen amount is increased. This table shows the simulation coefficients are practically constant as the free BSA amount increases, which is reasonable if the proposed reaction scheme is true.

The average kinetics binding parameters are constant in all simulation processes provided that the self-association of BSA molecules is considered. If it is not taken into account, these average parameters are not constant as the amount of antigen is increased. On the other hand, an IgG molecule could react only with a dimeric BSA molecule due to its size. However, the simulation of the experimental data from a reaction mechanism that considers an only FabBSA binding does not allow a good fit. Therefore, it is possible to say that IgG molecules only interact with free BSA and not with dimers and higher aggregates.

Self-association of albumin is a well-established phenomenon, where monomers and oligomers are in dynamical equilibrium.[35] This formation of oligomeric protein structures determines and regulates protein function[36] and improves protein stability.[37] Thus, the affinity of the BSA dimer for some ligands is lower than that of the BSA monomer.[35] BSA aggregates formation requires at least conformational changes at tertiary structure.[38] These changes modify the mechanism of recognition of proteins because this has a strong dependency on quaternary structures.[39] Furthermore, BSA aggregates at neutral pH present amyloidal properties with a unique kinetic stability.[40] Therefore, it is possible to confirm that the assumption of IgG molecules only interacting with free BSA and not with dimers and higher aggregates is acceptable.

The estimated self-association constant for BSA is 10^7 M^{-1}, about 100 times larger than that reported in 3-(*N*-morpholino)-propanesulfonic acid buffer (pH 5.8).[35] This difference could be due to changes of the specific experimental conditions, PBS (pH = 7.4), because the BSA aggregation pathway is mainly regulated by protein−solvent interactions modulated by pH.[41,42] At acid pH (pH ≅ 5, close to the isoelectric point), there is a fast formation of amorphous aggregates mainly mediated by hydrophobic interactions in the absence of secondary structure changes.[42] However, there is a formation of smaller aggregates when moving away from the isoelectric point, which is marked by secondary structure changes.[43] According to the value of the self-association constant determined in this work and taking into account the high BSA concentration in the blood plasma (around 600 μM), it should be mainly dimeric in this medium.

Results (Table 2) indicate that the total concentration of immobilized immunoglobulin, $N_{Pweak,0}$, is 0.12 mol m^{-3} at these experimental conditions, which is equivalent to an average degree of immobilization of IgG about 5%. This degree of immobilization is calculated considering the IgG theoretical structure[44] and the dimensions of the sensor chip surface. The estimated value agrees with short immobilization times,[45] such as the immobilization process carried out here. Furthermore, results clearly show how two Fab fragments have different association constants ($k_{1,1} \neq k_{2,1}$), although they are structurally identical. This agrees with the fact that the two binding sites for neonatal Fc receptor on Fc or IgG_1 have significantly different affinities.[46]

All simulation error is focused on the values of the polarizability volume per mole for species *i* (α_i) and the height change of the captured ligand (such as antibody or other macromolecule) due to its binding to the receptor *i* (such as antigen or other ligand) (d_i), which incorporates well the effect of system fluctuation on experimental measurement. Thus, it is possible to find more accurate values for average kinetic binding parameters. These will allow the response of oriented IgG-free BSA interaction, under different experimental conditions, to be better predicted. Because of the system fluctuations, the analysis of the α_i and d_i values may be carried out only considering average values. The average α_i values are about 0.5 m^3/mol and similar for all complexes proposed, which is logical because all complexes consist of a large IgG molecule and BSA smaller molecules. Although the polarizability volume depends on geometries of particles on the sensor surface,[48] the theoretical value of this parameter is estimated here considering both the BSA and the IgG molecules as jellium spheres and rejecting the molecules needed to anchor the IgGs on the sensor surface. Thus, the polarizability is related directly to the volume of the studied

dx.doi.org/10.1021/jp301953z | J. Phys. Chem. B 2012, 116, 5679−5688

Table 2. Parameters Calculated from the Simulations of DPI Data Obtained While the Oriented IgG-Free BSA Interaction Is Happening in PBS (pH = 7.4)[a]

[BSA], μg/mL	$k_{1,1}$, $m^3\ mol^{-1}\ s^{-1}$	$k_{1,2}$, s^{-1}	$k_{2,1}$, $m^3\ mol^{-1}\ s^{-1}$	$k_{2,2}$, s^{-1}	refractive index plot				thickness plot			
					$\alpha_{P_{weak}}$, $m^3\ mol^{-1}$	$\alpha_{P_{weak}*L}$, $m^3\ mol^{-1}$	$\alpha_{P_{tight}*L}$, $m^3\ mol^{-1}$	$\alpha_{P_{2,weak}*L}$, $m^3\ mol^{-1}$	$d_{P_{weak}*L}$, Å	$d_{P_{tight}*L}$, Å	$d_{P_{2,weak}*L}$, Å	$d_{P_{2,tight}*L}$, Å
0.10	1.5×10^5	7.0×10^{-3}	1.0×10^4	7.0×10^{-3}	0.5075	0.5056	0.5093	0.5060	43.55	43.55	63.15	82.75
0.50	1.5×10^5	7.0×10^{-3}	1.0×10^4	7.0×10^{-3}	0.5088	0.5075	0.5070	0.5070	43.55	43.55	67.51	117.59
1.00	1.5×10^5	7.0×10^{-3}	1.0×10^4	7.0×10^{-3}	0.5096	0.5080	0.5083	0.5070	43.55	43.55	78.39	143.72
2.00	1.5×10^5	7.0×10^{-3}	1.0×10^4	7.0×10^{-3}	0.5088	0.5080	0.5085	0.5067	43.55	43.55	69.68	154.61
5.00	1.5×10^5	7.0×10^{-3}	1.0×10^4	7.0×10^{-3}	0.5070	0.5080	0.5085	0.5065	43.55	43.55	87.10	152.43
A[b]	1.5×10^5	7.0×10^{-3}	1.0×10^4	7.0×10^{-3}	0.5083	0.5074	0.5083	0.5066	43.55	43.55	73.17	130.22
								0.5055				

[a]The estimated self-association constant for BSA molecules is $10^7\ M^{-1}$, and $N_{Pweak,0}$ is 0.12 mol m^{-3}. [b]A is arithmetic mean.

molecules,[47] and so the orders of magnitude of α_i can be estimated from $\alpha_{BSA} = 0.03\ m^3/mol$.[48] The theoretical values of α_i are about 0.1 m^3/mol and agree with the DPI values. Accordingly, this strong approximation shows the value estimated here is possible. Nevertheless, this topic will be the subject of future research using quantum approximation algorithms.

The experimental results (Table 2) give d_i values for P_{weak*L} and $P_{tight*L}$ of about 43 Å. Thus, and as BSA molecules are prolate ellipsoids where the polar axis (140 Å) is larger than the equatorial axes (40 Å),[44,49] this value of 43 Å indicates that the first Fab fragment may recognize mainly the BSA molecule by its polar axis (Scheme 1).

Scheme 1. Proposed Reaction Scheme

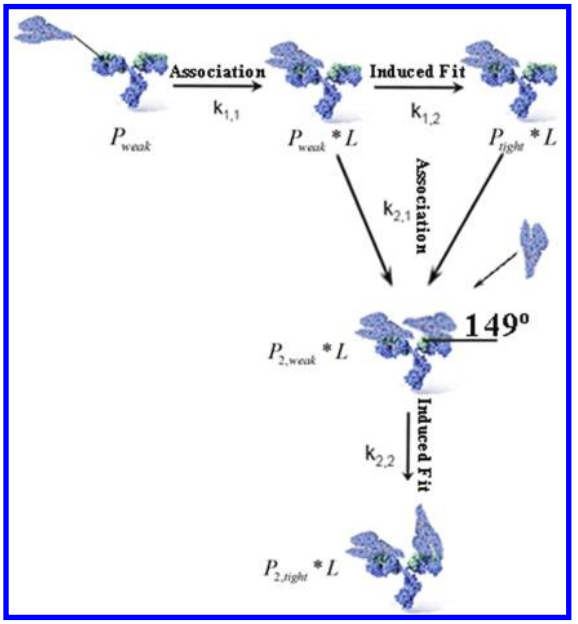

On the other hand, the average d_i value for the $P_{2,weak*L}$ complex is 73.17 Å. The second binding BSA molecule would be tilted at an angle about 149° with respect to the plane defined through the two epitope binding Fab regions of each IgG molecule, which is parallel to the sensor chip surface due to the oriented disposition of antibody molecules. Also, the average d_i value for the $P_{2,tight*L}$ complex is equal to 130.22 Å, which means that the second binding BSA molecule is recognized by the second Fab fragment via its equatorial axis. The location of the two binding BSA molecules with respect to the two paratopes of each IgG molecule is beyond question due to the experimental values of d_i. Other possible locations of the BSA molecules would not reproduce the experimental values.

X-ray crystallography reveals that the distance between the two binding sites of IgG molecules is around 120 Å.[44] Thus, if the first binding BSA molecule is recognized by its polar axis such as it is measured experimentally, the second molecule could not be located in this way due to steric effects. It should be recognized by the second Fab fragment via its equatorial axis. Consequently, and as both Fab fragments are identical, one of the logical reasons to explain the empirical data is that of there being steric effects, which favor one molecular recognition region over the other, thus changing the second association constant. The first biomolecular binding reorientates the following one; that is, the second BSA molecule tries to be recognized by its polar axis, but it may be recognized by its equatorial axis due to steric effects.

dx.doi.org/10.1021/jp301953z | J. Phys. Chem. B 2012, 116, 5679−5688

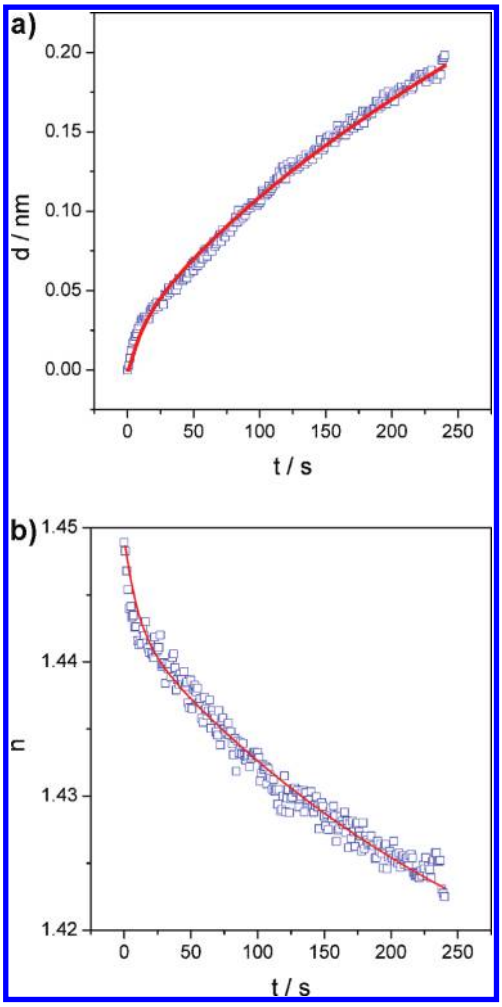

Figure 3. Curves of refractive index and thickness versus time during the oriented mouse IgG monoclonal antibody-free BSA interaction at [BSA] = 1.00 μg/mL in PBS (pH = 7.4) and at 20 °C. The continuous lines are the simulations from the following kinetic parameters: $k_{1,1} = 1.5 \times 10^2$ m^3 mol^{-1} s^{-1}, $k_{1,2} = 1.0 \times 10^{-1}$ m^3 mol^{-1} s^{-1}, $k_{2,1} = 1.0 \times 10^2$ m^3 mol^{-1} s^{-1}, $k_{2,2} = 7.0 \times 10^{-3}$ m^3 mol^{-1} s^{-1}, $N_{Pweak,0} = 0.12$ mol m^{-3}, $\alpha_{Pweak} = 0.534$ m^3 mol^{-1}, $\alpha_{Pweak*L} = 0.420$ m^3 mol^{-1}, $\alpha_{Ptight*L} = 0.510$ m^3 mol^{-1}, $\alpha_{P2,weak*L} = 0.450$ m^3 mol^{-1}, $\alpha_{P2,tight*L} = 0.480$ m^3 mol^{-1}, $d_{Pweak*L} = 108.88$ Å, $d_{Ptight*L} = 39.20$ Å, $d_{P2,weak*L} = 80.57$ Å, and $d_{P2,tight*L} = 143.72$ Å. (a) Curve of the adlayer thickness. (b) Curve of the refractive index.

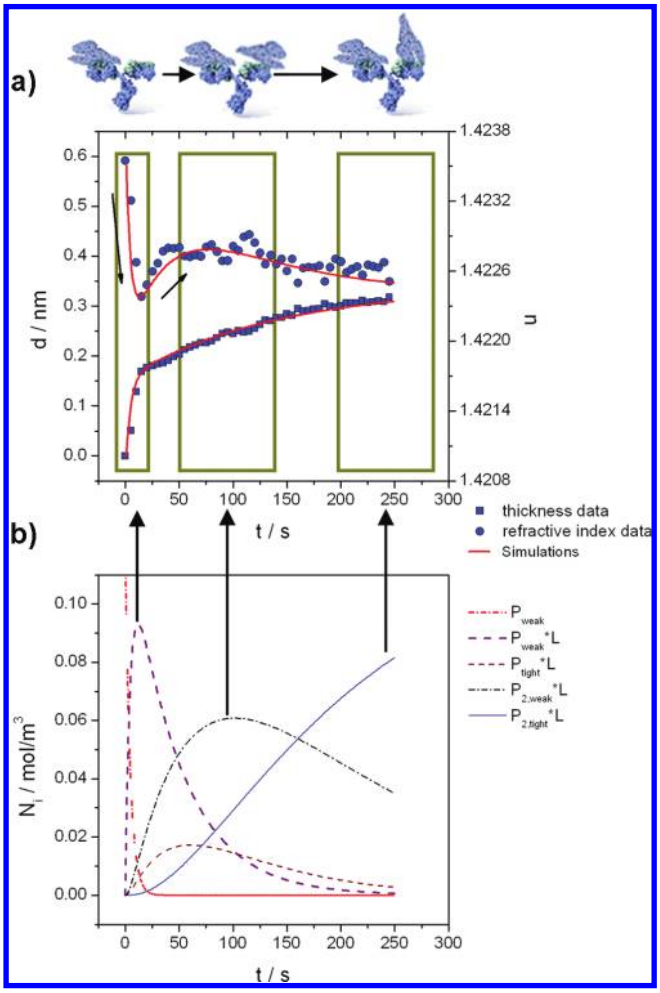

Figure 4. (a) Curves of refractive index and thickness versus time during the oriented rabbit IgG polyclonal antibody-free BSA interaction at [BSA] = 0.10 μg/mL in PBS (pH 7.4) and at 20 °C. (b) Time evolution of the reactive species. All plots show only one point for every five points that are measured.

The experimental results allow one to depict the exact location of the reactant molecules during the binding process, drawing the full reaction scheme (Scheme 1). Accordingly, it is possible to say that the induced fit model may be the one that best describes the oriented IgG-free BSA interaction because the conformational selection model establishes an intermediate state without BSA molecules, $d_i = 0$. This result is in accordance with the fact that the rearrangements in the variable domains of Fab are interpreted as an induced fit mechanism required to secure a stable complex.[50,51]

This novel approach is a powerful tool for rigid distinction between the induced fit and conformational selection models. The relative importance of the two pathways is determined not by comparing rate constants (a common misconception), but instead by comparing the structural aspects of the interaction.

At this point, the model may be tested experimentally for a monoclonal immunoglobulin to confirm, without a doubt, the results obtained so far. Here, the results are verified by studying the mouse IgG monoclonal antibody-free BSA interaction, in which the IgG is anchored on the sensor surface in a oriented manner. If the model is true, it may simulate what is physically happening during the time evolution of the interaction of any IgG with free BSA molecules. The kinetic parameters can depend on the kind of studied IgG, but the interaction mechanism may always be the same. Thus, Figure 3 shows how the proposed mathematical model provides a very good simulation view for the mouse IgG monoclonal antibody-free BSA interaction. The trends of the thickness and refractive index plots are well simulated by means of these equations, according to the residual variances of the thickness and refractive index, 1.27×10^{-5} nm^2 and 8.13×10^{-7}, respectively. The correct fit of these results implicates that the proposed interaction model is true. The IgG-free BSA interaction happens by the induced fit model, where the two Fab fragments of IgG molecules have different association constants due to steric effects. Furthermore, this accordance implicates an unexpected homogeneous behavior despite the appreciable biological heterogeneity of the rabbit IgG polyclonal antibody, which reconfirms previous hypotheses.

As commented above, the kinetic parameters may depend on the kind of IgG that is being studied because the IgG molecules of different animals differ structurally, although they have in common the basic aspects of structure. So, the parameters that depend on the structures interacting, such as kinetic constants and the polarizability volumes per mole, should be reasonably different. However, the

dx.doi.org/10.1021/jp301953z | J. Phys. Chem. B 2012, 116, 5679−5688

parameters that depend on the location of the two binding BSA molecules with respect to the capture antibody may be very similar. Accordingly, Figure 3 shows how the kinetic constants and the polarizability volumes per mole of all reactive species are different, whereas the d_i values are very similar both when the reactive species is a monoclonal antibody as when it is polyclonal. Furthermore, the polarizability volumes of the monoclonal and polyclonal IgG complexes have also the same order of magnitude, because both IgG structures may be similar. Therefore, the conclusions related to this location are reconfirmed without a doubt.

The proposed approach can explain why the signals change the way they do in terms of the binding events. Figure 4 shows the deconvolution of empirical data of the oriented IgG-free BSA interaction obtained from mathematical model deduced above. In this case, it can be easily seen how the experimental results are characterized by the prevalence of three different reactive species over time. For the refractive index changes, the trends are a fast decrease of large amplitude due to the progressive proliferation of the P_{weak*L} molecules that are at the sensor (solid)−liquid interface, then a slower increase with smaller amplitude because of the increase of $P_{2,weak*L}$ molecules at this interface, followed by a decrease at longer time as a result of the proliferation of $P_{2,tight*L}$. For thickness data, the phases could be also understood as an increase of the amount of the P_{weak*L}, $P_{2,weak*L}$, and $P_{2,tight*L}$ complexes over time. Thus, the proposed reaction scheme easily gives physical meaning to experimental data.

From these results, researchers should be in a position to understand and predict antibody−antigen interaction for a variety of endogenous and exogenous antigens. In this regard, this should prove to be a valuable tool in biomolecular recognition studies to monitor all species involved in the reaction mechanism, allowing the full reaction scheme drawing.

CONCLUSIONS

Biomolecular interactions are typically monitored to model relevant aspects of reality, in a way that supports processes requiring this information. Accordingly, a tool by modeling the protein−protein interaction by dual polarization interferometry is here developed. The tremendous potential of this modeling is tested by studying the anti-BSA Immunoglobulin G-free BSA interaction, in which the IgG is oriented anchored on a sensing surface. Thus, the kinetic and structural aspects of this interaction are quantified. The kinetic studies hardly ever insist on the derivation of conformational information, which plays a key role on the reaction kinetics. Thus, as our power to investigate protein reactions increases, so has our inherent understanding of these mechanisms. This tool makes possible a search in new areas, even when there is no high-resolution structural information about reactive species (e.g., the in situ characterization of intermediate states).

The tool allows a rigid distinction between the possible reaction mechanisms of ligand binding coupled to conformational changes in macromolecules: conformational selection or induced fit. The relative importance of the two pathways is determined by comparing the structural aspects of the interaction. So the proposed mathematical modeling allows the exact location of the two binding BSA molecules with respect to the capture antibody to be depicted, avoiding the use of X-ray crystallography and its consequent disadvantages.

The oriented IgG-free BSA interaction takes place by means of the induced fit model. The first Fab fragment may recognize mainly BSA molecules by its polar axis, so reorienting itself following binding due to steric effects. Thus, the second binding BSA molecule would be located initially tilted at an angle about 149° with respect to the plane defined through the two paratopes of each IgG molecule. This molecule then would be reoriented to be recognized by the second Fab fragment via its equatorial axis. This information could be valid for antibodies behavior in solution, because if the second antigen molecule is large, it would not be bound at the best recognized paratope but a secondary one, thus avoiding steric hindrance.

The proposed tool also allows the empirical data points to be deconvoluted, so characterizing the reaction intermediates without the need to isolate them, something that may not be possible, in many cases. This deconvolution method is in fact sufficient to discriminate a majority of the species present in a multicomponent solution, for example, blood serum. A single measurement may allow all species involved in the studied interaction mechanism to be characterized by this modeling, which could be exploited regarding biosensors development, pharmacokinetics, drug discovery, biomaterials, etc. This discrimination capability also allows the polarizability volume of nonisolated species to be calculated. These unknown values are usually calculated on the basis of the quantum model. Hence, it could provide experimental results to corroborate the theoretical data, thus confirming the conclusions derived from them.

The conformational kinetic study carried out here could provide a basis for modifications of the protein to carry therapeutic or diagnostic agents, and create smaller proteins with enhanced binding activities for a variety of applications. The generation of engineered forms (chimeric, humanized, human) of antibodies and the exploration of novel modifications to improve the pharmacokinetics represent exciting areas of biotechnological research in which it could be very useful to apply the developed methodology. This advance provides a window into many areas of active research at the interface of chemistry and biology.

AUTHOR INFORMATION

Corresponding Author

*E-mail: amaquieira@qim.upv.es.

Notes

The authors declare no competing financial interest.

ACKNOWLEDGMENTS

This research was funded through project Feder CTQ2010-15943 (CICYT, Spain), GVA ACOMP-2009/650, and GVA Prometeo 2010/008. D.G.-R. acknowledges his position in the "Ramon y Cajal" Program (Spanish Ministry of Economy and Competitiveness).

REFERENCES

(1) Nath, N.; Chilkoti, A. *Anal. Chem.* **2004**, *76*, 5370−5378.
(2) James, L. C.; Roeversi, P.; Tawfik, D. S. *Science* **2003**, *299*, 1362−1367.
(3) Boehr, D. D.; Nussinov, R.; Wright, P. E. *Nat. Chem. Biol.* **2009**, *5*, 789−796.
(4) Koshland, D. E., Jr. *Proc. Natl. Acad. Sci. U.S.A.* **1958**, *44*, 98−104.
(5) Berger, C.; Weber-Bornhauser, S.; Eggenberger, J.; Hanes, J.; Pluckthun, A.; Bosshard, H. R. *FEBS Lett.* **1999**, *450*, 149−153.
(6) Leder, L.; Berger, C.; Bornhauser, S.; Wendt, H.; Ackermann, F.; Jelesarov, I.; Bosshard, H. R. *Biochemistry* **1995**, *34*, 16509−16518.
(7) Foote, J.; Milstein, C. *Proc. Natl. Acad. Sci. U.S.A.* **1994**, *91*, 10370−10374.
(8) Ross, A. M.; Zhang, D.; Deng, X. P.; Chang, S. L.; Lahann, J. *Anal. Chem.* **2011**, *83*, 874−880.
(9) Jin, G.; Tengvall, P.; Lundstrom, I.; Arwin, H. *Anal. Biochem.* **1995**, *232*, 69−72.

(10) Wu, J.; Balasubramanian, S.; Kagan, D.; Manesh, K. M.; Campuzano, S.; Wang, J. *Nat. Commun.* **2010**, *1*, 36.
(11) Zourob, M.; Mohr, S.; Fielden, P. R.; Goddard, N. J. *Lab Chip* **2005**, *5*, 772−777.
(12) Yu, J. S.; Trnavsky, M.; McDonagh, C.; MacCraith, B. D. *Biosens. Bioelectron.* **2010**, *25*, 1344−1349.
(13) Chancellor, T. F.; Russell, R. J.; Dravid, V.; Lele, T. P. *Biotechnol. Prog.* **2008**, *24*, 89−95.
(14) Andersson, K.; Karlsson, R.; Loefaas, S.; Franklin, G.; Haemaelaeinin, M. D. *Exp. Opin. Drug Discovery* **2006**, *1*, 439−446.
(15) Cross, G. H.; Reeves, A. A.; Brand, S.; Popplewell, J. F.; Peel, L. L.; Swann, M. J.; Freeman, N. J. *Biosens. Bioelectron.* **2003**, *19*, 383−390.
(16) Lin, S.; Lee, C. K.; Wang, Y. M.; Huang, L. S.; Lin, Y. H.; Lee, S. Y.; Sheu, B. C.; Hsu, S. M. *Biosens. Bioelectron.* **2006**, *22*, 323−327.
(17) Terry, C. J.; Popplewell, J. F.; Swann, M. J.; Freeman, N. J.; Fernig, D. G. *Biosens. Bioelectron.* **2006**, *22*, 627−632.
(18) Popplewell, J. F.; Swann, M. J.; Freeman, N. J.; McDonnell, C.; Ford, R. C. *Biochim. Biophys. Acta, Biomembr.* **2007**, *1768*, 13−20.
(19) Mashaghi, A.; Swann, M.; Popplewell, J.; Textor, M.; Reimhult, E. *Anal. Chem.* **2008**, *80*, 3666−3676.
(20) Sonesson, A. W.; Callisen, T. H.; Brismar, H.; Elofsson, U. M. *Colloids Surf., B* **2007**, *54*, 236−240.
(21) Swann, M. J.; Peel, L. L.; Carrington, S.; Freeman, N. J. *Anal. Biochem.* **2004**, *329*, 190−198.
(22) Daghestani, H. N.; Day, B. W. *Sensors* **2010**, *10*, 9630−9646.
(23) Lane, T. J.; Fletcher, W. R.; Gromally, M. V.; Johal, M. S. *Langmuir* **2008**, *24*, 10633−10636.
(24) Mashaghi, A.; Swann, M.; Popplewell, J.; Textor, M.; Reimhult, E. *Anal. Chem.* **2008**, *80*, 3666−3676.
(25) Edmondson, S.; Vo, C. D.; Armes, S. P.; Unali, G. F. *Macromolecules* **2007**, *40*, 5271−5278.
(26) Lin, S. M.; Lee, C. K.; Lin, Y. H.; Lee, S. Y.; She, B. C.; Tsai, J. C.; Hsu, S. M. *Biosens. Bioelectron.* **2006**, *22*, 715−721.
(27) Hubert, R. *Klin Woechenschr.* **1980**, *58*, 1217−1231.
(28) Roux, K. *Int Arch. Allergy Immunol.* **1999**, *120*, 85−99.
(29) Lorentz, H. A. *Ann. Phys.* **1880**, *9*, 641−665.
(30) Lorenz, L. V. *Ann. Phys.* **1880**, *11*, 70−103.
(31) Ogawa, T.; Kazuo, S. *J. Chem. Eng. Data* **1976**, *21*, 33−35.
(32) Anderson, G. K. *Int. J. Thermophys.* **1997**, *18*, 699−717.
(33) Lee, L.; Johnston, A. P. R.; Caruso, F. *Biomacromolecules* **2008**, *9*, 3070−3078.
(34) Wilson, M. B.; Nakane, P. K. In *Inmunofluorescence and Related Staining Techniques*; Knapp, W., Holubar, H., Wick, G., Eds.; Elsevier: Amsterdam, 1978; pp 215−214.
(35) Levi, V.; Gonzalez-Flecha, F. *Biochim. Biophys. Acta* **2002**, *1599*, 141−148.
(36) Kovalsky, O.; Lung, F. D.; Roller, P. P.; Fornace, A. J. J. *J. Biol. Chem.* **2001**, *276*, 39330−39339.
(37) Bowie, J. U. *Curr. Opin. Struct. Biol.* **2001**, *11*, 397−402.
(38) Vetri, V.; D'Amico, M.; Foderà, V.; Leone, M.; Ponzoni, A.; Sberveglieri, G.; Militello, V. *Arch. Biochem. Biophys.* **2011**, *508*, 13−24.
(39) Ito, H. O.; Ueda, T.; Hashimoto, Y.; Imoto, T.; Koga, T. *Cell. Mol. Life Sci.* **1997**, *53*, 51−60.
(40) Holm, N.; Jespersen, S.; Thomassen, L.; Wolff, T.; Sehgal, P.; Thomsen, L.; Christiansen, G.; Andersen, C.; Knudsen, A.; Otzen, D. *Biochim. Biophys. Acta* **2007**, *1774*, 1128−1138.
(41) San Biagio, P. L.; Bulone, D.; Emanuele, A.; Palma, M. U. *Biophys. J.* **1996**, *70*, 494−499.
(42) Vetri, V.; Librizzi, F.; Leone, M.; Militello, V. *Eur. Biophys. J.* **2007**, *36*, 717−725.
(43) Militello, V.; Vetri, V.; Leone, M. *Biophys. Chem.* **2003**, *105*, 133−141.
(44) Harris, L. J.; Skaletsky, E.; McPherson, A. *J. Mol. Biol.* **1998**, *275*, 861−872.
(45) Zengin, A.; Caykara, T. *Appl. Surf. Sci.* **2011**, *257*, 2111−2117.
(46) Schuck, P.; Radu, C. G.; Ward, E. S. *Mol. Immunol.* **1999**, *36*, 1117−1125.
(47) Apell, P. S.; Sabin, J.; Trickey, S. B.; Oddershede, J. *Int. J. Quantum Chem.* **2002**, *86*, 35−39.
(48) Noto, M.; Keng, D.; Teraoka, I.; Arnold, S. *Biophys. J.* **2007**, *92*, 4466−4472.
(49) Bloomfield, V. *Biochemistry* **1966**, *5*, 684−789.
(50) Smirnov, I.; Carletti, E.; Kurkova, I.; Nachon, F.; Nicolet, Y.; Mitkevich, V. A.; Debat, H.; Avalle, B.; Belogurov, A. A.; Kuznetsov, N.; et al. *Proc. Natl. Acad. Sci. U.S.A.* **2011**, *108*, 15954−15959.
(51) Rini, J. M.; Schulze-Gahmen, U.; Wilson, I. A. *Science* **1992**, *255*, 959−965.